Journal of Materials Processing Technology 213 (2013) 1743–1752

Contents lists available at SciVerse ScienceDirect

Journal of Materials Processing Technology

journal homepage: www.elsevier.com/locate/jmatprotec

'Herringbone' defect formation in planar-flow melt spinning

B.L. Cox [a,*], P.H. Steen [b]

[a] Exponent, Inc., 4580 Weaver Parkway, Suite 100, Warrenville, IL 60555, USA
[b] School of Chemical and Biomolecular Engineering, Cornell University, Ithaca, NY 14853, USA

ARTICLE INFO

Article history:
Received 19 February 2013
Received in revised form 18 April 2013
Accepted 19 April 2013
Available online 2 May 2013

Keywords:
Planar-flow spin casting
Planar-flow melt spinning
Defect formation
Herringbone defect
Crosswave defect
Casting

ABSTRACT

A short-wavelength, periodic feature (≈1 mm) similar in appearance to a herringbone pattern appeared on ribbon produced at high rates (≈10 m/s) by the planar-flow process. These marks corresponded to a high-frequency (≈10 kHz) disturbance to the process stream. Observations of herringbone formation came from ribbon profilometry, customized nozzle tests and high-speed meniscus imaging. These observations were compared against observations of the 'crosswave' feature formation which were subject to prior study. It is demonstrated here that herringbone marks, in contrast to the crosswave marks, were mainly influenced by the substrate motion of translation. Herringbone formation is also reported to have correlated with the pinning of the liquid puddle at the nozzle edge.

1. Introduction

Planar-flow melt spinning (PFMS) is a single-stage casting process characterized by rapid solidification into thin ribbon. Local variations in product thickness can result from disturbances to the melt fluid flow or to the heat transport. For example, Theisen et al. (2010) showed that changes to the resistance to fluid flow yielded variations in ribbon thickness and Byrne et al. (2007) and Sundararajan and Thomas (2008) showed experimentally and through numerical simulations, respectively, that heat transfer interruptions had a similar but more localized effect on the ribbon product. Short-wavelength or high-frequency, periodic variations in thickness were the focus of this study.

Narasimhan (1979) patented the continuous casting method now known as PFMS. PFMS received considerable attention during the late 1970s and 1980s as a technique to continuously cast amorphous metals commonly called metallic glasses. Kavesh (1978) described the principles of fabrication of metallic glasses and identified PFMS as an attractive method, owing to its high cooling rates that achieve up to 10^8 K/s under ideal conditions. In the 1980s and 1990s PFMS became the leading method for the manufacture of metallic glasses. This commercialization notwithstanding, PFMS has not achieved its early promise in part because the process is difficult to control. The appearance of casting marks limits the alloys that can be successfully cast and, for those that can be cast, the speed of processing.

Interest worldwide in large scale PFMS reemerged recently. Much of the recent demand for metallic glasses comes from higher-efficiency energy conversion devices. Hasegawa and Azuma (2008) reviewed the many induction-based electromagnetic applications that would benefit from PFMS-produced metallic glasses. Hasegawa (2000) also identified the importance of amorphous soft magnetic alloys in the latest generation of high-efficiency cores for power-distribution transformers. Herzer (2003) described the benefits of amorphous alloy ribbon in his survey of magneto-acoustic surveillance devices. Li et al. (2011) report using PFMS to cast from a 3-ton capacity crucible pilot facility. In addition, for reasons of productivity rather than microstructure, Hahn et al. (2009) has sought to commercialize a PFMS variant to continuously cast silicon wafers for solar-cell applications.

The PFMS apparatus used here, Fig. 1a, comprised a sealed graphite crucible surrounded by an induction heating coil, seated above a moving substrate. The liquid metal in the crucible was pushed by argon gas overpressure out of a rectangular nozzle slot, of cross-stream and streamwise dimensions W and B, respectively. The typical casts reported here had dimensions of width $W = 50$ mm and slot breadth $B = 3$ mm, an aspect ratio that made the process essentially two-dimensional. After emerging from the nozzle slot and contacting the rotating wheel, the molten metal froze and was spun off as solid ribbon product. The ribbon width normally followed the slot width W to within 2% (or 1 mm), as typical of PFMS.

As it solidifies, the molten metal in PFMS is held by surface tension in the gap between nozzle and wheel in a long and thin region

* Corresponding author. Tel.: +1 6306587523.
E-mail addresses: bcox@exponent.com (B.L. Cox), phs7@cornell.edu (P.H. Steen).

0924-0136/$ – see front matter © 2013 Elsevier B.V. All rights reserved.
http://dx.doi.org/10.1016/j.jmatprotec.2013.04.009

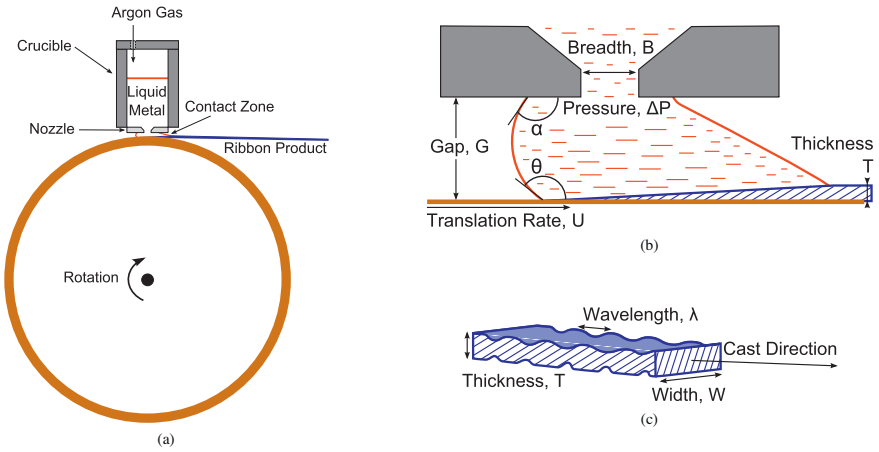

Fig. 1. Sideview sketch of (a) casting machine and of (b) contact-zone or 'puddle' showing liquid metal (dashed), solidified metal (hatched), and substrate wheel beneath (solid). Also, (c) a sketch of a portion of ribbon exhibiting a periodic defect is shown. Liquid metal was pushed by pressure ΔP through a rectangular nozzle of breadth B and width W, $W \gg B$, making the contact-zone features essentially uniform into the page. The nozzle was spaced a distance G above the substrate which translates at a speed U. Solidified ribbon of thickness T exited the contact zone moving with the wheel at speed U. Upstream contact-lines between the melt, gas, and nozzle, and between the melt, gas and substrate, had contact angles of α and θ, respectively. Contact zone, as sketched, is not to scale was of order 1×20 mm, in actuality. Ribbon typically formed of width W, and often exhibiting a defect of wavelength λ (also not to scale).

called the contact zone or 'puddle', Fig. 1b. The meniscus holding the melt is subject to motion, which can lead to thickness variations that appear as casting lines or marks that span the ribbon width, Fig. 1c. Casting lines in PFMS have been previously discussed. Carpenter and Steen (1992) summarized a variety of ribbon surface textures. Praisner et al. (1995) reported 'dimpled' and 'striated' lines that form in a 50/50 Pb–Sn alloy. They found that these lines could be avoided by keeping the liquid Stefan number within a specified range. This Stefan number avoidance criteria was met for all of the Al 7%Si casts performed in the present study, and no dimpled or striated lines were observed.

Byrne et al. (2006a) focused specifically on the 'crosswave' lines identified previously. By correlating the meniscus frequency and the spacing of the 'crosswave' lines, meniscus vibrations were identified as the source of the features. To the naked eye, the crosswave (CW) defect appears as a continuous mark from one side of the ribbon to the other, Fig. 2a. Byrne et al. (2006b) reported a window in (scaled) parameter space for the appearance of the CW. This window occurred within a larger window in parameter space where successful casting occurred (see also, Appendix A).

In the present study, cross-stream marks called 'herringbone' were compared against the superficially similar 'crosswave' lines studied by Byrne et al. (2006a). Herringbone (HB) lines are similar to CW lines but shorter in wavelength, Fig. 2b. HB lines were first reported by Carpenter and Steen (1992) and later mentioned by Praisner et al. (1995) and Byrne et al. (2006a). Theisen (2007) observed that, like CW, the HB frequency scaled with the capillary frequency $(\sigma/\rho G^3)^{1/2}$, but shifted upward. Here σ is the molten metal surface tension, ρ the liquid density and G the nozzle-wheel gap, Fig. 1b. It was also reported that HB tends to occur at lower overpressure than does CW. It was speculated that this low overpressure resulted in a puddle that was pinned at the nozzle slot. Despite this prior work, the mechanism of formation of HB has remained largely an open question.

Details about the process and experimental methodology are provided in Section 2. In Section 3, two classes of disturbances are defined, a classification which will distinguish HB frow CW. In Section 4, standard characterizations contrast HB against CW. Building on this comparison, Section 5 uses a dimensional argument to motivate the functional dependence of observed wavelengths. When the data is plotted in these dimensionless variables, wavelengths for HB are seen to be influenced by wheelspeed, and hence HB differs in an essential way from CW formation.

2. Apparatus and experimental methods

The contact zone was bounded above by the nozzle face, below by the moving substrate, and on the sides by the molten metal/gas meniscus, Fig. 1b. A rectangular slot of breadth B and width W was machined into the molded nozzle, which was positioned a distance G above the wheel substrate. Pressure ΔP forced the molten metal through the slot and into contact with the translating substrate where it solidified. The substrate was a copper-beryllium wheel whose rate-of-rotation was set beforehand and then recorded as a linear velocity U throughout the cast. The gap G between the bottom of the nozzle and the substrate was set before a cast began and G typically decreased as the cast progressed, a consequence of heat being absorbed by the wheel which caused it to expand toward the nozzle (cf. Theisen et al., 2010). The resulting deviation from the initial gap was measured by a capacitance gauge which provided an instantaneous gap-value throughout the cast. The gap values were subsequently averaged over the cast and reported as G (Appendix B).

Prior to casting, an initial pressure of argon gas was applied to evacuate oxygen, water vapor, and other potentially reactive gases, after which the crucible was sealed. That initial pressure was maintained constant until the cast began, at which time the pressure was ramped to compensate for the loss of hydrostatic head as the metal reservoir depleted. The reported pressure ΔP was the time-average of the sum of the applied and hydrostatic pressures experienced at the nozzle inlet (cf. Fig. 1b). After a cast, the ribbon product was cut into segments whose width and mass were measured. The average thickness T of each segment was thereby calculated. For casts exhibiting a periodic casting line, an average wavelength λ was manually calculated for each segment. Cast-average values of data collected for HB casts appear in Appendix B; CW data was taken from Byrne et al. (2006a).

High speed images of the contact zone were recorded. Images were captured between 3000 and 50,000 fps, with resolutions up to 6 μm per pixel using a 90 mm macro lens. The zone was backlit to highlight the upstream meniscus (USM) and downstream meniscus (DSM) during a cast. Direct visual observation of the USM at the nozzle face showed it as either 'unpinned', Fig. 3b (top right), in which case it could move along the face, or 'pinned', Fig. 3b (top left), in which case it remained fixed at the nozzle slot. Video analysis also allowed simultaneous observation of the motion of both